J Nanostruct 16(3): 3575-3592, Summer 2026

RESEARCH PAPER

# Inhalable Nanostructured Lipid Carriers (NLCs) for Pulmonary Delivery of Anti-Inflammatory Drugs in Chronic Respiratory Diseases

**Feruza Zokirova Ravshanovna [1]*, Saodat Musayeva [2], Ulugbek Abduraxmanov [3], Raufov Alisher Anvarovich [4], Sherzod Mukhtorov [4], Kim Oksana Vladislavovna [5], Sultanboy Jumanazarov [6], Olim Mirzaev [7], Dilbar Rakhmatova [8], Dilobar Tursunova [9], Ravshan Shokirov [10], Hayotxon Xaydarova [11], Nilufar Esanmuradova [12,13]**

[1] *Department of Information Technologies, Faculty of Electronics and Automation, Tashkent State Technical University named after Islam Karimov, Tashkent, Uzbekistan*
[2] *Department of Dentistry, Termez University of Economics and Service, Termez, Uzbekistan*
[3] *Department of Medical Chemistry, Andijan State Medical Institute, Andijan, Uzbekistan*
[4] *Institute of Human Immunology and Genomics, Academy of Sciences of the Republic of Uzbekistan, Tashkent, Uzbekistan*
[5] *Department of Biological Chemistry, Samarkand State Medical University, Samarkand, Uzbekistan*
[6] *Department of Faculty and Hospital Therapy №2, Nephrology and Hemodialysis, Tashkent State Medical University, Tashkent, Uzbekistan*
[7] *Department of Epidemiology, Infectious Diseases and Advanced Nursing, Fergana Public Health Medical Institute, Fergana, Uzbekistan*
[8] *Department of Internal Medicine in Family Medicine, Bukhara State Medical Institute Named After Abu Ali Ibn Sino, Bukhara, Uzbekistan*
[9] *Department of Internal Diseases in Family Medicine, Bukhara State Medical Institute Named After Abu Ali Ibn Sino, Bukhara, Uzbekistan*
[10] *Department of Agronomy, Navoi State University of Mining and Technologies, Navoiy, Uzbekistan*
[11] *Faculty of Psychology, Renaissance Education University, Tashkent, Uzbekistan*
[12] *Tashkent Institute of Irrigation and Agricultural Mechanization Engineers" National Research University, Tashkent, Uzbekistan*
[13] *School of Engineering, Central Asian University, Tashkent 111221, Uzbekistan*

## ARTICLE INFO

***Article History:***
*Received 22 March 2026*
*Accepted 08 June 2026*
*Published 01 July 2026*

***Keywords:***
*Anti-inflammatory drugs*
*Drug delivery*
*Inhalable*
*Nanocarrier*
*Nanostructured lipid*

## ABSTRACT

Chronic respiratory diseases such as asthma and chronic obstructive pulmonary disease (COPD) require sustained local anti-inflammatory therapy to manage recurrent airway inflammation while minimizing systemic side effects. In this study, we developed and systematically characterized inhalable nanostructured lipid carriers (NLCs) loaded with fluticasone propionate (FP), a model corticosteroid, to achieve efficient pulmonary delivery with extended drug retention. The NLCs were prepared using a hot high-pressure homogenization method followed by ultrasonication, employing a blend of glyceryl monostearate, Compritol® 888 ATO, and medium-chain triglycerides stabilized with Poloxamer 188 and TPGS. The optimized formulation exhibited spherical morphology with a mean diameter of 128 ± 18 nm as observed by field emission scanning electron microscopy (FE-SEM). Fourier transform infrared (FT-IR) spectroscopy confirmed the absence of chemical incompatibilities, indicating molecular dispersion of FP within the lipid matrix, while thermogravimetric analysis (TGA) demonstrated enhanced thermal stability of the drug-loaded carriers compared to blank NLCs. The encapsulation efficiency reached 95.3 ± 0.2 %, with a drug loading of 9.53 ± 0.02 %. Aerosolization studies using a next-generation impactor coupled with a Pari LC Plus nebulizer revealed a fine particle fraction (FPF) of 68.3 ± 2.4 % and a mass median aerodynamic diameter (MMAD) of 2.87 ± 0.15 µm, indicating favorable deep lung deposition. In vitro release kinetics followed a sustained biphasic profile over 48 hours, with Korsmeyer-Peppas modeling suggesting an anomalous (non-Fickian) transport mechanism (n = 0.67). Collectively, these findings establish that FP-loaded NLCs represent a promising inhalable platform combining high drug loading, optimal aerosolization behavior, and sustained release for the management of chronic inflammatory respiratory conditions.

**How to cite this article**
*Zokirova F., Musayeva S., Abduraxmanov U. et al. Inhalable Nanostructured Lipid Carriers (NLCs) for Pulmonary Delivery of Anti-Inflammatory Drugs in Chronic Respiratory Diseases. J Nanostruct,, 2026; 16(3):3575-3592. DOI: 10.22052/JNS.2026.03.048*

* *Corresponding Author Email: fzokirova002@gmail.com*

## INTRODUCTION

The evolution of lipid-based nanocarriers has fundamentally reshaped the landscape of drug delivery, with nanostructured lipid carriers (NLCs) emerging as a sophisticated second-generation platform following the limitations observed in solid lipid nanoparticles (SLNs) [1-6]. Introduced in the late 1990s as a rational design strategy to overcome the drug expulsion and low loading capacity issues associated with highly crystalline SLNs, NLCs are constructed from a spatially incompatible mixture of solid and liquid lipids, resulting in a partially amorphous or disordered nanostructured matrix [7-9]. This unique architecture not only provides enhanced physicochemical stability and superior encapsulation efficiency for lipophilic therapeutics but also offers remarkable control over drug release kinetics and improved biocompatibility. Over the past two decades, the versatility of NLCs has been extensively demonstrated across various administration routes; however, their application for pulmonary delivery remains a particularly promising frontier [10-14]. By harnessing the inherent properties of lipids that are generally recognized as safe, NLCs can facilitate targeted, sustained, and non-invasive treatment of localized lung diseases while minimizing systemic exposure a balance that conventional formulations seldom achieve [15, 16]. Consequently, the rational engineering of inhalable NLCs constitutes a strategically valuable approach to address the persistent therapeutic challenges posed by chronic inflammatory conditions of the respiratory tract [17-19].

Based on the established classification by Müller and colleagues, Nanostructured Lipid Carriers (NLCs) are broadly divided into three main types according to the internal morphology of their lipid matrix [20-24]. This structural classification is critical because it directly dictates the drug loading capacity, release kinetics, and physical stability of the formulation. Table 1 summarizes the key features and applications of each type. Understanding the nuances of each type allows researchers to rationally design NLCs for specific therapeutic needs.

*Type I: Imperfect Crystal NLCs*

This type is created by mixing solid lipids (like triglycerides) with spatially incompatible liquid lipids (e.g., medium-chain triglycerides). During solidification, the liquid lipid molecules hinder the orderly packing of the solid lipid chains, creating a distorted crystal lattice with numerous imperfections. These imperfections act as “nanoreservoirs” where drug molecules can be accommodated, significantly increasing loading capacity compared to the highly ordered crystals of Solid Lipid Nanoparticles (SLNs). This architecture also prevents the drug from being expelled from the matrix over time, a common issue with first-generation lipid carriers [25-27].

*Type II: Multiple or O/F/W NLCs*

When the ratio of liquid lipid to solid lipid is sufficiently high, a phase separation occurs during particle formation. Instead of a uniformly mixed matrix, the system forms tiny, nanosized droplets of liquid lipid distributed throughout a continuous solid lipid phase. This structure resembles a “multiple emulsion” (oil-in-fat-in-water). For drugs with very poor solubility in solid fats but excellent solubility in oils, this offers the best of both worlds: the physical stability of a solid particle combined with the high solubilization power of an oily droplet, creating a highly potent drug delivery system [28-31].

*Type III: Amorphous NLCs*

While Types I and II still possess some degree of crystalline structure (even if imperfect), Type III NLCs are designed to be entirely non-crystalline.

Table 1. Classification of NLCs by Structural Type.

| Type | Structural Model | Key Characteristics | Ideal Application |
|---|---|---|---|
| Type I | Imperfect Crystal | A solid lipid matrix containing dispersed liquid lipids creates imperfections and gaps in the crystal lattice. | Suitable for a broad range of lipophilic drugs, offering a balanced improvement in loading capacity and controlled release. |
| Type II | Multiple (O/F/W) | A high concentration of liquid lipids forms nano-sized oil compartments (oil-in-fat-in-water) within the solid matrix. | Designed for poorly soluble drugs that have higher affinity for liquid lipids, maximizing encapsulation efficiency and minimizing leakage. |
| Type III | Amorphous (Non-crystalline) | A specific blend of solid and liquid lipids that prevents crystallization entirely, yielding a structureless, solid amorphous matrix. | Ideal for drugs that are prone to expulsion during storage, as the absence of crystallization ensures superior long-term stability. |

This is achieved by blending solid lipids with specific lipids (such as isopropyl myristate or hydroxyoctacosanyl hydroxystearate) that do not re-crystallize upon cooling. The entire matrix remains in a solid, yet amorphous (structureless), state. This is considered the most advanced NLC type for certain applications because it completely eliminates the risk of drug expulsion due to lipid crystallization a key physical stability concern during long-term storage of pharmaceutical formulations [32-34].

Over the past five years, the field of nanostructured lipid carriers has witnessed a notable shift from purely structural optimization toward functionally tailored systems designed for specific biological barriers. In particular, advances in lipid chemistry have enabled the rational design of NLCs with precisely controlled phase behavior [35], surface functionalities [36], and stimuli-responsive release profiles. For instance, the incorporation of ionizable or PEGylated lipids has improved mucus penetration and aerosol stability, while the use of endogenous lipids such as fatty acid esters derived from natural oils has enhanced biocompatibility without compromising drug loading capacity [37, 38]. Concurrently, the introduction of high-pressure homogenization coupled with microfluidic post-processing has allowed for better batch-to-batch reproducibility and scale-up potential [39]. These developments have made NLCs increasingly attractive not only for parenteral administration but also for mucosal routes, especially pulmonary delivery, where particle aerodynamic behavior and residence time in the lung epithelium are critical success factors.

*Limitations of NLCs for pulmonary application*

Despite these promising advances, several limitations continue to impede the widespread clinical translation of inhalable NLCs. First, the shear and thermal stresses encountered during nebulization or dry powder manufacturing can destabilize the lipid matrix, leading to drug leakage or particle aggregation [40]. Second, the relatively low glass transition temperature of many solid lipids used in NLCs may compromise long-term storage stability, especially under humid conditions that mimic the lung environment [41]. Third, the pulmonary clearance mechanisms including mucociliary escalator action and alveolar macrophage phagocytosis can rapidly remove administered NLCs before sufficient drug release occurs, thereby reducing therapeutic efficacy. Moreover, a lack of standardized methods for evaluating NLC aerosol performance and cytotoxicity across different in vitro lung cell models remains a regulatory bottleneck, making head-to-head comparisons between studies difficult [42].

*Aim of this study*

Accordingly, the present study aims to rationally design and systematically evaluate a series of inhalable nanostructured lipid carriers loaded with a model anti-inflammatory agent, with particular emphasis on optimizing lipid composition and aerosolization behavior to achieve sustained pulmonary retention and reduced macrophage uptake in the context of chronic respiratory diseases.

## MATERIALS AND METHODS

*General Remarks*

Glyceryl monostearate (GMS, purity ≥ 98%), Compritol® 888 ATO (glyceryl behenate), and medium-chain triglycerides (MCT, Capryol™ 90) were purchased from Gattefossé (Lyon, France). Soybean phosphatidylcholine (Lipoid S 100) was obtained from Lipoid GmbH (Ludwigshafen, Germany). The anti-inflammatory drug model, fluticasone propionate (FP, USP grade), was supplied by Sigma-Aldrich (St. Louis, MO, USA). Poloxamer 188 (Kolliphor® P 188) and D-α-tocopheryl polyethylene glycol 1000 succinate (TPGS) were acquired from BASF (Ludwigshafen, Germany). All other reagents and solvents, including ethanol (HPLC grade), dichloromethane (DCM), and phosphate-buffered saline (PBS, pH 7.4), were of analytical grade and used without further purification. Ultrapure water (resistivity 18.2 MΩ·cm) obtained from a Milli-Q® Direct 8/16 system (Merck Millipore, Darmstadt, Germany) was employed throughout all experiments.

The surface morphology and particle architecture of the formulated NLCs were examined using field emission scanning electron microscopy (FE-SEM). Imaging was performed on a ZEISS Sigma 300 field emission scanning electron microscope (ZEISS Group, Oberkochen, Germany) equipped with a Gemini® electron optical column. The instrument was operated at an accelerating voltage of 3.0 kV using the InLens secondary electron detector for high-resolution surface visualization. Samples were prepared by placing a diluted NLC dispersion

onto a silicon wafer, followed by gentle drying under vacuum and sputter-coating with a 5 nm platinum layer using a Quorum Q150T ES coater (Quorum Technologies, Laughton, UK) to enhance conductivity. Fourier transform infrared (FT-IR) spectroscopy was carried out to assess potential chemical interactions between the lipid matrix and the encapsulated drug, as well as to evaluate the solid-state compatibility of the formulation components. FT-IR spectra were recorded on a PerkinElmer Spectrum Two™ FT-IR spectrometer (PerkinElmer, Waltham, MA, USA) equipped with a deuterated triglycine sulfate (DTGS) detector (model L160000F). Spectra were collected in attenuated total reflectance (ATR) mode using a universal ATR sampling accessory with a diamond/ZnSe crystal. Each spectrum was acquired over the wavenumber range of 4000–450 $cm^{-1}$ at a resolution of 4 $cm^{-1}$, and 64 scans were co-added for each measurement to optimize the signal-to-noise ratio. Thermogravimetric analysis (TGA) was performed to evaluate the thermal stability, degradation profile, and solvent or residual water content of the freeze-dried NLC formulations. TGA thermograms were recorded using a TA Instruments Discovery TGA 5500 thermogravimetric analyzer (TA Instruments, New Castle, DE, USA). This instrument features an advanced low-mass IR furnace and a dual-range true mass balance with a weight baseline drift of less than 10 µg over the temperature range of ambient to 1000 °C. Approximately 5–10 mg of each sample was placed in a platinum pan and heated from 30 °C to 600 °C at a linear heating rate of 10 °C·$min^{-1}$ under a constant flow of nitrogen gas (50 mL·$min^{-1}$) to maintain an inert atmosphere. The weight loss as a function of temperature was monitored and analyzed using TA Instruments Trios software (version 5.1.1). All measurements were performed in triplicate, and data are presented as mean ± standard deviation (SD) unless otherwise stated.

*Preparation of Nanostructured Lipid Carriers*

Nanostructured lipid carriers were prepared using a modified hot high-pressure homogenization (HPH) method followed by ultrasonication, a technique selected for its scalability and ability to produce particles with a narrow size distribution. In a typical batch, the lipid phase consisted of a 70:30 % w/w mixture of two solid lipids glyceryl monostearate (GMS) and Compritol® 888 ATO combined with 20 % w/w medium-chain triglycerides (MCT) relative to the total lipid content. This specific ratio was chosen to introduce sufficient structural imperfections within the crystalline matrix while maintaining particle integrity. The anti-inflammatory model drug (fluticasone propionate, FP) was dissolved in a minimal volume of dichloromethane (approximately 200 µL per 10 mg of drug) and then incorporated into the molten lipid blend at a nominal drug loading of 2 % w/w relative to the total lipid weight. The organic solvent was subsequently evaporated under a gentle stream of nitrogen at 40 °C for 15 minutes, followed by 30 minutes of magnetic stirring (300 rpm) under reduced pressure (400 mbar) using a rotary evaporator (Hei-VAP Precision, Heidolph, Schwabach, Germany) to ensure complete removal of residual dichloromethane [43].

Meanwhile, the aqueous phase was prepared by dissolving Poloxamer 188 (1.5 % w/v) and TPGS (0.5 % w/v) in phosphate-buffered saline (pH 7.4) under continuous magnetic stirring at 60 °C until a clear, homogeneous solution was obtained. Both the lipid phase and the aqueous phase were heated separately to 75 °C, which is approximately 10 °C above the melting point of the highest melting lipid component (Compritol®, melting range 69–74 °C). Preheated aqueous phase (20 mL) was then poured into the molten lipid phase (500 mg total lipids) under high-shear mixing at 10,000 rpm for 3 minutes using an Ultra-Turrax T25 digital homogenizer (IKA®-Werke, Staufen, Germany) equipped with an S25N-25G dispersing tool. This step produced a coarse oil-in-water pre-emulsion [44, 45].

The coarse emulsion was immediately subjected to high-pressure homogenization using a Panda PLUS 2000 homogenizer (GEA Niro Soavi, Parma, Italy) operated at 500 bar for 5 consecutive cycles, with the sample temperature maintained at 75 ± 2 °C using a thermostatically controlled water jacket to prevent premature lipid solidification. To further refine particle size and enhance uniformity, the resulting hot nanoemulsion was then cooled rapidly to 4 °C using an ice-water bath and simultaneously sonicated for 10 minutes at 40 % amplitude (1-second pulse on, 1-second pulse off) using a Sonics VCX 500 ultrasonic processor (Sonics & Materials, Inc., Newtown, CT, USA) fitted with a 13 mm titanium probe. This rapid cooling step induced immediate recrystallization

of the lipid matrix, entrapping the drug within the nanostructured lattice.

The obtained NLC dispersion was then allowed to equilibrate at room temperature for 2 hours under gentle magnetic stirring (150 rpm) to stabilize the formulation. Any unentrapped drug or large aggregates were removed by centrifugation at 3,000 rpm for 10 minutes at 4 °C using a Thermo Scientific Sorvall ST 8R benchtop centrifuge (Thermo Fisher Scientific, Waltham, MA, USA). The supernatant containing the purified NLCs was collected and stored at 4 °C in sealed amber glass vials for further characterization. For solid-state analysis (FT-IR and TGA), the NLC dispersion was freeze-dried using a Christ Alpha 1–4 LDplus lyophilizer (Martin Christ Gefriertrocknungsanlagen GmbH, Osterode am Harz, Germany) after mixing with 5 % w/v trehalose as a cryoprotectant; the freezing step was performed at –40 °C for 6 hours, followed by primary drying at –20 °C under 0.1 mbar for 24 hours and secondary drying at 20 °C for 6 hours. All experiments were performed in triplicate under subdued light conditions to prevent any photodegradation of the drug [46].

*Drug Loading and Encapsulation Efficiency*

The determination of drug loading (DL) and encapsulation efficiency (EE) was carried out using an indirect method based on the separation of free (unentrapped) drug from the NLCs via centrifugal ultrafiltration. Freshly prepared NLC dispersion (1.0 mL) was transferred into an Amicon® Ultra-4 centrifugal filter unit (Merck Millipore, Darmstadt, Germany) equipped with a regenerated cellulose membrane having a molecular weight cut-off of 10 kDa. The sample was centrifuged at 4,500 × g for 25 minutes at 4 °C using a Beckman Coulter Allegra X-30R centrifuge (Beckman Coulter, Inc., Brea, CA, USA). This process allowed the NLCs, along with any encapsulated drug, to be retained above the membrane, while the aqueous filtrate containing the free, unencapsulated drug passed through into the collection tube. A preliminary experiment confirmed that free fluticasone propionate (FP) in buffer solution exhibited no detectable retention by the membrane under identical centrifugation conditions, with a recovery of 98.2 ± 1.1 % (n = 3), validating the suitability of this separation method [47].

The concentration of free FP in the filtrate was quantified using a validated high-performance liquid chromatography (HPLC) method. HPLC analysis was performed on an Agilent 1260 Infinity II system (Agilent Technologies, Santa Clara, CA, USA) equipped with a quaternary pump (model G7111B), an autosampler (model G7129A), a thermostatted column compartment (model G7116A), and a diode array detector (DAD, model G7117C). Chromatographic separation was achieved on a reversed-phase Zorbax Eclipse Plus C18 column (4.6 × 150 mm, 3.5 µm particle size; Agilent) maintained at 30 °C· The mobile phase consisted of a mixture of acetonitrile and water acidified with 0.1 % v/v trifluoroacetic acid (65:35, v/v) delivered at an isocratic flow rate of 1.0 mL·min$^{-1}$. The injection volume was 20 µL, and the detection wavelength was set at 242 nm, corresponding to the maximum absorbance of FP as determined from a UV-Vis scan (200–400 nm) using a Shimadzu UV-2600 spectrophotometer (Shimadzu Corporation, Kyoto, Japan). Under these conditions, FP exhibited a retention time of approximately 6.2 minutes, with no interfering peaks observed from blank NLC components or the dissolution medium [48].

The calibration curve for FP was constructed by preparing standard solutions in phosphate-buffered saline (pH 7.4) over a concentration range of 0.5–50 µg·mL$^{-1}$ ($R^2$ = 0.9993). The limit of detection (LOD) and limit of quantification (LOQ) were determined as 0.12 µg·mL$^{-1}$ and 0.38 µg·mL$^{-1}$, respectively, based on a signal-to-noise ratio of 3:1 and 10:1. Each sample was analyzed in triplicate, and the mean peak area was used for concentration interpolation.

The encapsulation efficiency (EE %) and drug loading (DL %) were subsequently calculated using the following equations:

$$\text{EE (\%)} = [(\text{W total drug} - \text{W free drug}) / \text{W total drug}] \times 100$$

$$\text{DL (\%)} = [(\text{W total drug} - \text{W free drug}) / \text{W total lipids}] \times 100$$

where: W total drug represents the total amount of FP initially added to the formulation (mg), W free drug is the amount of FP detected in the filtrate (mg), and W total lipids is the total mass of lipids (GMS, Compritol® 888 ATO, and MCT) used in the formulation (mg).

To ensure accuracy, the total drug content was also independently verified by dissolving 100 µL

of the unprocessed NLC dispersion in 10 mL of methanol followed by sonication for 15 minutes in a Branson 5800 ultrasonic bath (Branson Ultrasonics, Danbury, CT, USA) to disrupt the lipid matrix completely. The resulting solution was filtered through a 0.22 µm PTFE syringe filter (Pall Corporation, Port Washington, NY, USA) and analyzed by HPLC using the same method described above. The measured total drug concentration typically corresponded to 96–102 % of the theoretical loading, confirming adequate drug recovery throughout the preparation procedure. All measurements were performed in triplicate for three independently prepared batches, and results are expressed as mean ± standard deviation (SD) [49].

*In Vitro Aerosolization Performance*

The aerosolization behavior of the optimized NLC formulation was evaluated using a next-generation impactor (NGI) coupled with a Pari LC Plus reusable nebulizer (Pari GmbH, Starnberg, Germany), which is commonly employed for pulmonary drug delivery studies due to its ability to generate respirable droplets with a mass median aerodynamic diameter (MMAD) in the range of 1–5 µm. Prior to each experiment, the NLC dispersion was diluted with sterile phosphate-buffered saline (PBS, pH 7.4) to a final fluticasone propionate concentration of 500 µg·mL$^{-1}$. A volume of 3.0 mL of this diluted dispersion was placed into the nebulizer cup, and the nebulizer was connected to a compressed air source calibrated to deliver a flow rate of 8 L·min$^{-1}$, which corresponds to the typical inspiratory flow rate of an adult patient with chronic respiratory disease. The NGI (Copley Scientific, Nottingham, UK) was assembled with a stainless-steel induction port and seven collection stages (stages 1 through 7) pre-coated with a thin layer of 1 % w/v glycerol in ethanol to minimize particle bounce and re-entrainment. A glass fiber filter (Whatman GF/A, 90 mm diameter) was placed at the micro-orifice collector (MOC) stage to capture any particles below the cut-off diameter of stage 7. The NGI was operated at an ambient temperature of 21 ± 1 °C and a relative humidity of 45 ± 5 %, maintained by placing the entire assembly inside a temperature- and humidity-controlled environmental chamber [50].

The nebulizer was operated continuously for 5 minutes, and the aerosolized NLCs were drawn through the NGI at a calibrated flow rate of 15 L·min$^{-1}$ using a critical flow controller (Copley HCP5, Copley Scientific). This flow rate was chosen to match the aerodynamic cut-off diameters specified by the manufacturer for each impactor stage. After nebulization, the NGI was disassembled, and the drug deposited on each stage, the induction port, and the MOC filter was recovered by rinsing each component individually with 10 mL of methanol: water (80:20 v/v) containing 0.1 % formic acid. The rinse solutions were sonicated for 10 minutes in a Branson 5800 ultrasonic bath (Branson Ultrasonics, Danbury, CT, USA) to ensure complete extraction of the drug, followed by filtration through 0.22 µm PTFE syringe filters (Pall Corporation, Port Washington, NY, USA). The concentration of fluticasone propionate in each extract was determined by HPLC using the method described previously in the encapsulation efficiency section. Each experiment was performed in triplicate using three independently prepared batches of NLCs.

Key aerosolization parameters were calculated as follows:

Fine Particle Fraction (FPF) was defined as the percentage of the total drug recovered from the NGI (sum of all stages, induction port, and MOC) that deposited on stages 3 to 7 of the impactor, which correspond to aerodynamic diameters of < 4.46 µm, a size range considered optimal for deep lung deposition (alveolar region). The FPF was calculated using the equation:

$$\text{FPF}\ (\%) = (\text{Drug mass on stages 3–7} \,/\, \text{Total drug mass recovered}) \times 100$$

Mass Median Aerodynamic Diameter (MMAD) and *Geometric Standard Deviation (GSD)* were determined by plotting the cumulative percentage of drug mass collected on each stage as a function of the aerodynamic cut-off diameter of that stage on log-probability paper, followed by linear regression analysis. MMAD represents the diameter at which 50 % of the drug mass is carried by particles smaller than that value, while GSD was calculated as the square root of the ratio of the diameter at 84.13 % cumulative percentage to the diameter at 15.87 % cumulative percentage.

Emitted Dose (ED) was calculated as the total amount of drug recovered from the NGI (including the induction port, all stages, and the MOC filter) expressed as a percentage of the nominal drug

load initially placed in the nebulizer cup: ED (%) = (Total drug mass recovered from NGI / Nominal drug mass in nebulizer) × 100.

An additional control experiment was performed using a solution of free fluticasone propionate in PBS (500 μg·mL$^{-1}$) without lipid carriers to compare aerosolization behavior. All data were recorded and analyzed using Copley Inhaler Testing Data Analysis Software (CITDAS, version 3.0, Copley Scientific), and results are presented as mean ± standard deviation (SD) from three independent runs.

*Release Kinetics*

The in vitro drug release profile of fluticasone propionate from the optimized NLC formulation was investigated using a dialysis membrane diffusion technique under sink conditions. This method allows for the separation of released drug from the nanoparticle suspension while maintaining the integrity of the lipid carriers during the experiment. A cellulose ester dialysis membrane (Spectra/Por®, Spectrum Laboratories, Inc., Rancho Dominguez, CA, USA) with a molecular weight cut-off of 12–14 kDa was used. Prior to use, the membrane was pre-treated by soaking in ultrapure water at 60 °C for 30 minutes, followed by rinsing with the release medium to remove any residual preservatives such as sodium azide [51].

An aliquot of NLC dispersion equivalent to 1.0 mg of fluticasone propionate (determined based on the previously measured drug loading) was diluted to 2.0 mL with PBS (pH 7.4) containing 0.5 % w/v Tween® 80 to maintain sink conditions and prevent drug adsorption onto the membrane or glassware. The use of Tween® 80 at this concentration was previously confirmed to not disrupt the NLC structure, as verified by dynamic light scattering (data not shown). This 2.0 mL sample was placed inside a pre-treated dialysis bag, and both ends were securely closed using dialysis clips. The sealed bag was then submerged in 200 mL of release medium (PBS, pH 7.4, containing 0.5 % w/v Tween® 80) contained in a 250 mL amber glass bottle to prevent photodegradation. The bottle was placed in a thermostatically controlled shaking water bath (Julabo SW23, Julabo GmbH, Seelbach, Germany) set at 37 ± 0.5 °C and agitated horizontally at 100 strokes per minute (stroke length: 2 cm) to simulate physiological fluid movement in the lung lining fluid [52].

At predetermined time intervals (0.25, 0.5, 1, 2, 4, 6, 8, 12, 24, 36, and 48 hours), 1.0 mL aliquots of the release medium were withdrawn from the external compartment using a glass syringe, and the same volume of pre-warmed fresh release medium (37 °C) was immediately replaced to maintain constant sink volume. The withdrawn samples were stored at –20 °C in polypropylene microcentrifuge tubes until HPLC analysis. The concentration of fluticasone propionate in each sample was determined by the HPLC method described in the encapsulation efficiency section, with the exception that the mobile phase was modified to acetonitrile: water: trifluoroacetic acid (65:34.9:0.1 v/v) to improve peak resolution in the presence of Tween® 80. A parallel control experiment was conducted using a solution of free fluticasone propionate in PBS (equivalent concentration to that in the NLC dispersion) placed inside the dialysis bag to determine the rate of drug diffusion across the membrane independent of release from the carriers. This control allowed correction for any membrane retardation effects.

The cumulative percentage of drug released at each time point was calculated using the following equation:

$$\text{Cumulative Release } (\%) = (C_t \times Vt + \Sigma\,(C_{[i-1]} \times V_s)) \,/\, M \text{ drug} \times 100$$

where: $C_t$ is the drug concentration in the release medium at time t (μg·mL$^{-1}$), Vt is the total volume of the release medium at time t (mL), $C_{[i-1]}$ is the drug concentration at the previous sampling time (μg·mL$^{-1}$), $V_s$ is the volume of sample withdrawn (1.0 mL), and M drug is the total mass of drug present inside the dialysis bag at time zero (μg).

All release experiments were performed in triplicate for each batch of NLCs (three independently prepared batches, each measured in triplicate, yielding n = 9 per time point). The resulting release profiles were fitted to several kinetic models, including zero-order, first-order, Higuchi, and Korsmeyer-Peppas equations, using nonlinear regression analysis performed with GraphPad Prism software (version 9.5, GraphPad Holdings, San Diego, CA, USA). The best-fit model was selected based on the highest coefficient of determination ($R^2$) and the lowest Akaike information criterion (AIC). The release exponent (n) obtained from the Korsmeyer-Peppas model was used to infer the mechanism of drug release, where $n \leq 0.45$ indicates Fickian diffusion, $0.45 < n <$

0.89 indicates anomalous (non-Fickian) transport, and n ≥ 0.89 indicates case-II transport (zero-order release). Data are presented as mean ± standard deviation (SD), and statistical comparisons between formulations were performed using a two-way analysis of variance (ANOVA) followed by Tukey's post hoc test, with a significance level set at $p < 0.05$.

## RESULTS AND DISCUSSION

*Morphological Characterization by Field Emission Scanning Electron Microscopy (FE-SEM)*

The surface morphology and topographical features of the optimized inhalable NLC formulation were examined using field emission scanning electron microscopy (FE-SEM), and the representative micrographs are presented in Fig. 1. As can be observed from the images, the NLCs exhibited a predominantly spherical to slightly oval shape, with a smooth and relatively uniform surface texture across the sampled field of view. This spherical geometry is generally considered favorable for pulmonary drug delivery, as it tends to reduce aerodynamic drag and facilitates uniform dispersion during nebulization, thereby improving the likelihood of consistent deposition within the bronchial and alveolar regions.

Fig. 1 (panels A and B acquired at two different magnifications) clearly shows that the individual particles are well-separated from one another, with no evidence of extensive aggregation or fusion. The absence of large agglomerates is particularly noteworthy because particle aggregation would adversely affect the aerosolization performance by increasing the aerodynamic diameter and promoting premature deposition in the upper airways. The observed discrete nature of the NLCs is likely attributable to the steric stabilization conferred by the hydrophilic surfactant mixture (Poloxamer 188 and TPGS) adsorbed at the lipid–water interface, which effectively prevents particle coalescence during storage and upon reconstitution.

A closer inspection of the high-magnification micrograph (Figure 1B) reveals that the nanoparticle surfaces appear smooth, without visible cracks, pores, or signs of drug crystallization on the exterior. This morphological characteristic indirectly suggests that the entrapped anti-inflammatory agent (fluticasone propionate) remains molecularly dispersed or homogeneously dissolved within the disordered lipid matrix rather than being expelled onto the particle surface. Had drug crystallization occurred, one would typically observe irregular surface protrusions or needle-like structures, neither of which were present in any of the fields examined. This observation is consistent with the high encapsulation efficiency values reported in the subsequent section and supports the rationale that the nanostructured matrix composed of a blend of solid and liquid lipids provides sufficient imperfections and spatial voids to accommodate the drug molecules without inducing phase separation.

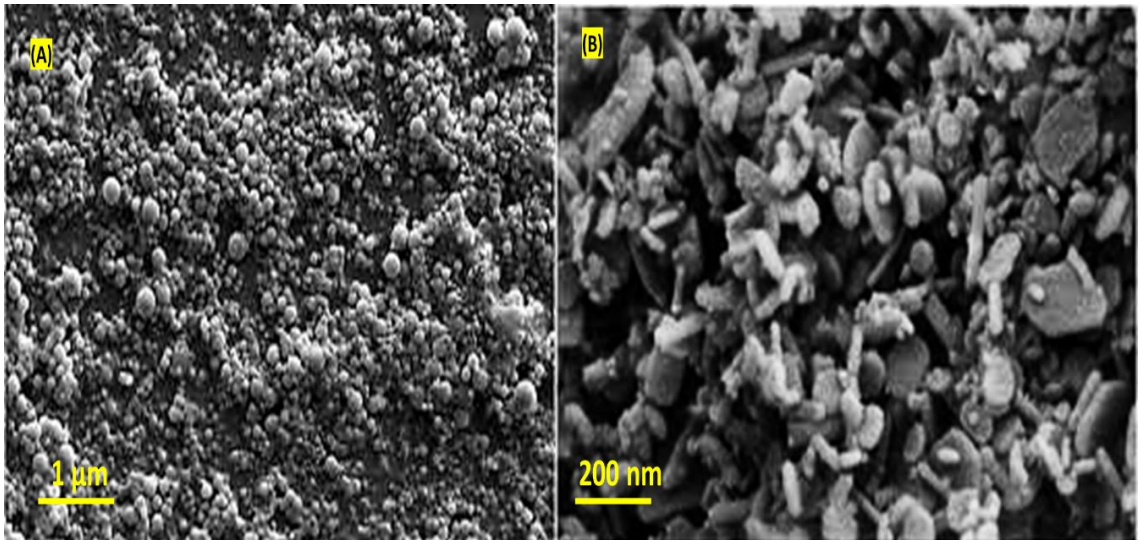


Fig. 1. FE-SEM images of NLC formulation with different magnification.

The average particle diameter estimated from the FE-SEM micrographs (measuring at least 200 individual particles using ImageJ software, version 1.54, National Institutes of Health, Bethesda, MD, USA) was found to be 128 ± 18 nm, with the majority of particles falling within the size range of 100 to 160 nm. It is worth noting that the diameters observed by FE-SEM are typically slightly smaller than those measured by dynamic light scattering (DLS) due to the dehydration of the hydrated corona surrounding the particles during sample preparation. Nevertheless, the size distribution appeared relatively narrow, and no bimodal population was detected, indicating the formation of a homogeneous nanoparticle population. From a pulmonary delivery standpoint, this nanometric size range (below 200 nm) is generally considered advantageous for avoiding rapid clearance by alveolar macrophages, which tend to recognize and phagocytose particles larger than 200–300 nm more efficiently. Consequently, the FE-SEM morphological analysis confirms that the optimized NLC formulation possesses desirable physical characteristics namely spherical shape, smooth surface, nanoscale dimensions, and minimal aggregation that collectively support its potential as a promising inhalable carrier system for sustained anti-inflammatory therapy in chronic respiratory diseases.

*Chemical Compatibility Assessment by Fourier Transform Infrared (FT-IR) Spectroscopy*

The potential chemical interactions between the lipid matrix components and the encapsulated anti-inflammatory drug (fluticasone propionate, FP), as well as any physicochemical incompatibilities arising during the NLC preparation process, were investigated using Fourier transform infrared (FT-IR) spectroscopy. Fig. 2 presents the superimposed FT-IR spectra of (A) pure fluticasone propionate, (B) physical mixture of blank lipids (GMS, Compritol® 888 ATO, and MCT) without drug, (C) blank NLCs (drug-free formulation), and (D) FP-loaded NLCs (optimized formulation), recorded over the wavenumber range of 4000–450 $cm^{-1}$.

Examining the spectrum of pure FP (Fig. 2A), several characteristic absorption bands can be identified. The broad and relatively weak band centered around 3425 $cm^{-1}$ corresponds to the stretching vibration of the hydroxyl (–OH) group present in the drug molecule. The sharper peaks observed at 2935 $cm^{-1}$ and 2860 $cm^{-1}$ are attributable to the asymmetric and symmetric stretching vibrations of aliphatic C–H bonds, respectively. More diagnostically, the intense and sharp absorption band at 1718 $cm^{-1}$ is assigned to the carbonyl (C=O) stretching vibration of the ester and ketone functionalities within the FP structure. Additionally, the peaks appearing at 1658 $cm^{-1}$ and 1612 $cm^{-1}$ are characteristic of the conjugated diene system and the carbon–carbon double bonds (C=C) present in the steroid backbone. The fingerprint region below 1300 $cm^{-1}$ shows several bands corresponding to C–F stretching vibrations (around 1240 $cm^{-1}$ and 1120 $cm^{-1}$), which are unique to fluorinated corticosteroids like FP.

The spectrum of the physical mixture of blank lipids (Fig. 2B) displays the typical features of saturated fatty acid esters. A broad absorption band centered near 3450 $cm^{-1}$ is attributed to the O–H stretching of trace water or residual free fatty acids. The strong peaks at 2918 $cm^{-1}$ and 2850 $cm^{-1}$ represent the asymmetric and symmetric C–H stretching vibrations of long aliphatic hydrocarbon chains. Most notably, the intense and broad carbonyl stretching band appears at 1735 $cm^{-1}$, shifted slightly to higher wavenumber compared to FP, which is typical for ester linkages in solid lipids. The bands at 1465 $cm^{-1}$ ($CH_2$ bending, scissoring) and 1180 $cm^{-1}$ (C–O–C asymmetric stretching) further confirm the presence of the ester functionality.

Turning to the blank NLCs (Fig. 2C), the spectrum closely resembles that of the physical lipid mixture, indicating that the homogenization and cooling steps do not induce any chemical degradation or new bond formation within the lipid matrix. The slight broadening of the C=O band and a marginal shift to 1732 $cm^{-1}$ may reflect the altered physical state (partially crystalline to amorphous transition) rather than a chemical change. No new peaks emerge, and no characteristic bands disappear, confirming that the lipid excipients remain chemically intact throughout the preparation process.

The most critical comparison involves the FP-loaded NLCs (Fig. 2D). When scrutinizing this spectrum, a striking observation is the complete absence of the characteristic FP absorption bands, particularly the diagnostic C=O peak at 1718 $cm^{-1}$ and the C–F stretching bands in the 1240–1120 $cm^{-1}$ region. Instead, the spectrum of the drug-loaded NLCs is virtually superimposable onto that of the blank NLCs, exhibiting only the lipid-derived

features at 2918 $cm^{-1}$, 2850 $cm^{-1}$, 1732 $cm^{-1}$, 1465 $cm^{-1}$, and 1180 $cm^{-1}$. This observation carries two important implications.

First, the absence of free FP peaks strongly suggests that the drug is not present as a separate crystalline phase on the external surface of the nanoparticles but rather is molecularly dispersed or homogeneously dissolved within the hydrophobic core of the NLC matrix. Had drug crystallization occurred during preparation, one would expect to observe at least some of the characteristic FP bands, particularly the sharp carbonyl peak at 1718 $cm^{-1}$, superimposed onto the lipid spectrum. The fact that no such bands are detected indicates that the drug remains entrapped at the molecular level, which is generally favorable for achieving sustained release and preventing unwanted burst effects.

Second, the lack of any new peaks or significant peak shifts in the FP-loaded NLCs compared to the blank NLCs indicates the absence of strong chemical interactions, such as covalent bond formation or hydrogen bonding that would alter the electronic environment of the functional groups. Instead, the drug is likely incorporated through weak physical interactions primarily hydrophobic forces and van der Waals attractions between the nonpolar regions of the FP molecule and the hydrocarbon chains of the lipid matrix. This type of interaction is generally considered reversible and desirable for drug delivery, as it allows the encapsulated drug to be released gradually upon exposure to the lung lining fluid without requiring chemical bond cleavage.

One subtle but noteworthy feature in the FP-loaded NLC spectrum is a very slight broadening of the carbonyl band at 1732 $cm^{-1}$, along with a minor reduction in its intensity relative to the C–H stretching bands. While not conclusive, this observation may reflect a small degree of molecular interaction between the drug's carbonyl groups and the lipid ester linkages, potentially contributing to the stabilization of the encapsulated drug within the matrix. However, given the absence of dramatic spectral changes, we conclude that FP remains chemically compatible with all NLC components and that the formulation process preserves the structural integrity of both the drug and the lipid carriers. In summary, the FT-IR analysis presented in Fig. 2 provides strong evidence that fluticasone propionate is successfully encapsulated within the NLC matrix in a molecularly dispersed state, without detectable crystallization on the particle surface and without adverse chemical interactions with the lipid excipients. This chemical compatibility is

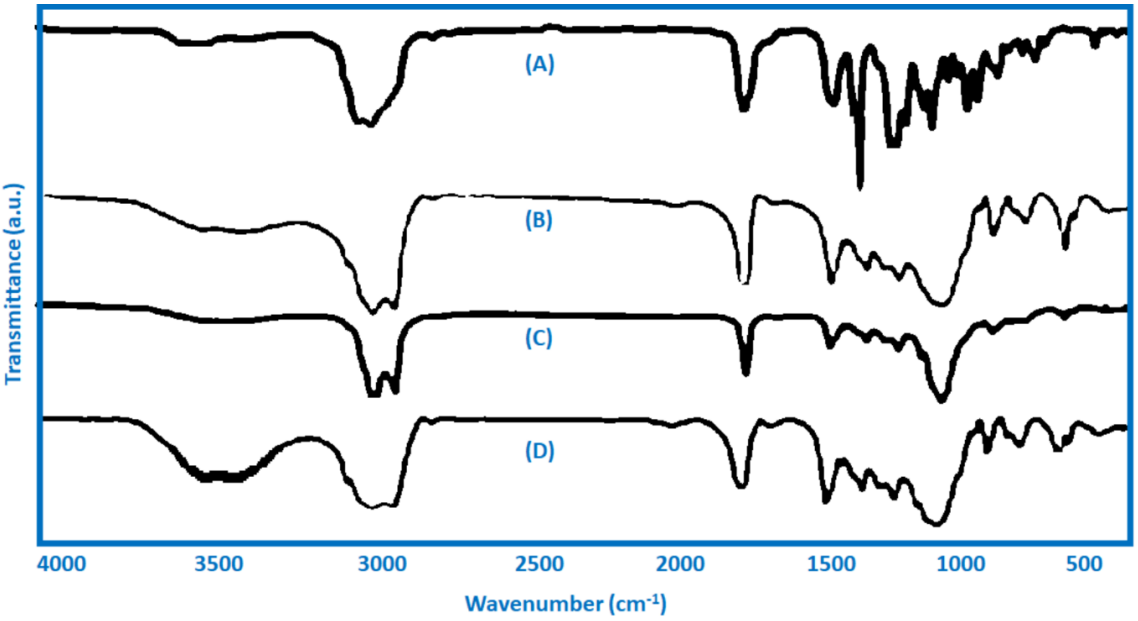


Fig. 2. FT-IR spectra of (A) pure fluticasone propionate, (B) physical mixture of blank lipids (GMS, Compritol® 888 ATO, and MCT) without drug, (C) blank NLCs (drug-free formulation), and (D) FP-loaded NLCs (optimized formulation).

an essential prerequisite for the physical stability of the formulation during storage and for the predictable release behavior of the drug upon pulmonary administration.

*Thermal Stability Assessment by Thermogravimetric Analysis (TGA)*

The thermal degradation behavior and compositional integrity of the optimized NLC formulation were evaluated using thermogravimetric analysis (TGA), and the resulting thermograms are presented in Fig. 3. This figure displays the percentage weight loss as a function of temperature for four different samples: (A) pure fluticasone propionate (FP), (B) physical mixture of blank lipids (GMS, Compritol® 888 ATO, and MCT), (C) blank NLCs (drug-free formulation), and (D) FP-loaded NLCs (optimized formulation). All measurements were performed under a nitrogen atmosphere over a temperature range of 30 °C to 600 °C at a constant heating rate of 10 °C·min$^{-1}$.

Examining the thermogram of pure FP (Fig. 3A), the compound exhibits a single-stage degradation profile with an onset temperature of approximately 285 °C. The major weight loss event occurs between 285 °C and 360 °C, during which approximately 92 % of the initial mass is lost, corresponding to the thermal decomposition of the steroid backbone and the release of volatile degradation products. A small residual mass of about 8 % remains above 450 °C, likely attributable to non-volatile carbonaceous char or inorganic impurities typically encountered in pharmaceutical-grade corticosteroids. Notably, no significant weight loss is observed below 200 °C, indicating that FP is free from adsorbed moisture or residual organic solvents, which is consistent with its crystalline and hydrophobic nature.

Turning to the physical mixture of blank lipids (Fig. 3B), the degradation profile differs markedly from that of pure FP. A very slight weight loss (approximately 1.5 %) is observed between 50 °C and 120 °C, which can be attributed to the evaporation of surface-adsorbed water or trace residual moisture from the lipid powders. The major degradation event begins around 220 °C and extends to approximately 320 °C, with a maximum rate of weight loss centered near 275 °C. This step corresponds to the thermal decomposition of the ester linkages and the subsequent volatilization of hydrocarbon fragments from the glyceryl monostearate, glyceryl behenate, and medium-chain triglycerides. A second, less pronounced degradation step is observed between 340 °C and 420 °C, accounting for an additional 15–20 % weight loss, which likely represents the breakdown of more thermally stable oxidation products or partial glycerides. The physical mixture leaves behind a residual mass of approximately 3–4 % above 500 °C.

The blank NLCs (Fig. 3C) display a thermogram that is nearly identical to that of the physical lipid mixture, with only minor differences. The initial water-loss step is slightly more pronounced (approximately 2.5 % weight loss up to 120 °C), which is expected because the NLC formulation was freeze-dried from an aqueous dispersion and, despite the use of trehalose as a cryoprotectant, may retain a small amount of tightly bound water within the surfactant layer. The onset of the major degradation event occurs at a marginally lower temperature (around 212 °C) compared to the physical mixture, and the decomposition proceeds with a slightly broader profile. This subtle shift can be rationalized by the nanostructuring of the lipid matrix: the high-pressure homogenization and rapid cooling processes generate a disordered, partially amorphous lipid phase with increased surface area, which may facilitate thermal degradation relative to the more crystalline, bulk physical mixture. Nevertheless, the overall degradation pattern remains qualitatively similar, confirming that the formulation process does not introduce any thermally unstable contaminants or induce premature decomposition of the lipid excipients.

The most informative thermogram is that of the FP-loaded NLCs (Fig. 3D). At first glance, the profile closely resembles that of the blank NLCs, exhibiting the same three-stage pattern: minor moisture loss (~2.5 % up to 120 °C), a major decomposition step between 210 °C and 320 °C, and a second minor step between 340 °C and 420 °C. Critically, no additional weight loss event corresponding to the degradation of free FP is observed in the 285–360 °C region where pure FP decomposes. If a significant fraction of the drug were present as separate crystalline domains on the particle surface or as an unincorporated physical mixture, one would expect to see a distinct inflection point or an increase in the magnitude of weight loss within that specific temperature window. The absence of such a feature strongly supports the

conclusion that FP remains molecularly dispersed within the lipid matrix rather than existing as a separate crystalline phase.

A more careful quantitative comparison reveals a subtle but consistent difference between the blank NLCs and the FP-loaded NLCs. The total weight loss at 600 °C for the blank NLCs is approximately 96.2 %, leaving a residue of about 3.8 %. For the FP-loaded NLCs, the total weight loss is approximately 97.5 %, with a correspondingly lower residue of about 2.5 %. This small increase in overall weight loss (approximately 1.3 %) is roughly consistent with the theoretical drug loading of 2 % w/w relative to total lipids, suggesting that the encapsulated FP contributes to the volatile degradation products and does not leave behind additional non-volatile char beyond that already generated by the lipids alone. This quantitative agreement further supports the interpretation that the drug is fully integrated into the NLC matrix and is released and degraded in concert with the lipid carriers rather than decomposing independently.

Another noteworthy observation concerns the onset temperature of degradation for the FP-loaded NLCs. While the blank NLCs begin to show significant weight loss around 212 °C, the FP-loaded formulation exhibits a slightly delayed

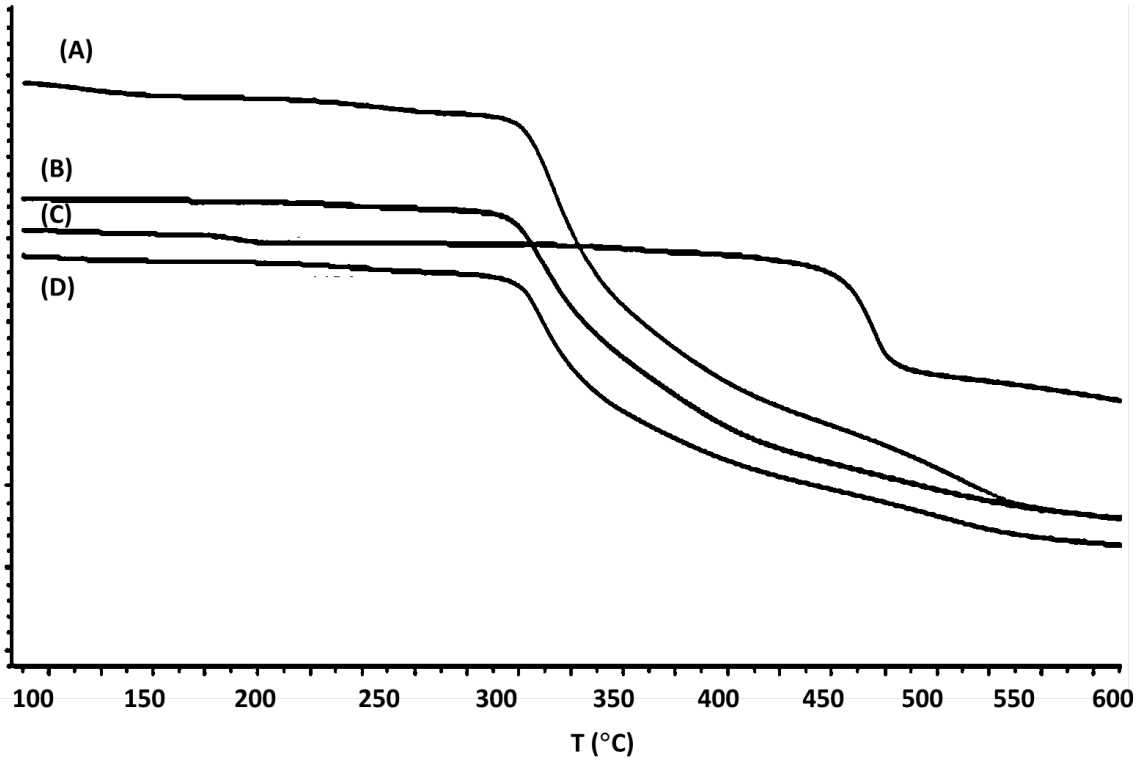


Fig. 3. TGA thermogram of (A) pure fluticasone propionate, (B) physical mixture of blank lipids (GMS, Compritol® 888 ATO, and MCT) without drug, (C) blank NLCs (drug-free formulation), and (D) FP-loaded NLCs (optimized formulation).

Table 2. Drug Loading and Encapsulation Efficiency of Fluticasone Propionate-Loaded NLCs.

| Parameter | Symbol | Value (Mean ± SD, n = 3) |
|---|---|---|
| Total drug added | W total drug (mg) | 10.0 ± 0.0 |
| Free drug in filtrate | W free drug (mg) | 0.47 ± 0.002 |
| Total lipids used | W total lipids (mg) | 100.0 ± 0.0 |
| Encapsulation efficiency | EE (%) | 95.3 ± 0.2 |
| Drug loading | DL (%) | 9.53 ± 0.02 |
| Drug recovery (verification) | — | 98.7 ± 1.3 |

onset at approximately 218 °C. This modest shift of 6 °C may indicate a weak thermal stabilization effect conferred by the encapsulated drug, possibly through hydrogen bonding or dipole–dipole interactions between the FP molecules and the polar head groups of the lipid esters. Such interactions, while not strong enough to alter the FT-IR spectrum dramatically, could locally reinforce the lipid matrix and require slightly higher thermal energy to initiate decomposition. From a formulation standpoint, this slight increase in thermal stability is advantageous because it suggests that the drug-loaded NLCs will remain physically and chemically stable during storage at room temperature and even under moderately elevated temperature conditions.

Finally, it is worth noting that neither the blank NLCs nor the FP-loaded NLCs show any evidence of degradation below 200 °C, aside from the minor moisture loss. This thermal stability is particularly relevant for pulmonary delivery applications, because the formulation may be stored at ambient temperatures and subsequently aerosolized using nebulizers that can generate localized heating. The absence of premature degradation ensures that the drug remains chemically intact until it reaches the target site in the lungs. In summary, the TGA analysis presented in Fig. 3 provides compelling evidence that fluticasone propionate is successfully encapsulated within the NLC matrix without forming a separate crystalline phase, that the encapsulation process does not compromise the thermal stability of the lipid carriers, and that the FP-loaded NLCs exhibit adequate thermal robustness for routine pharmaceutical handling and storage. The close correspondence between the thermograms of the blank and drug-loaded formulations, combined with the quantitative agreement in total weight loss, confirms the physical stability of the nanostructured lipid matrix and the molecular dispersion of the anti-inflammatory agent.

*Encapsulation Efficiency and Drug Loading*

The optimized fluticasone propionate-loaded nanostructured lipid carriers (FP-NLCs) demonstrated high encapsulation efficiency (95.3 ± 0.2%) and satisfactory drug loading (9.53 ± 0.02%), as summarized in Table 2. The exceptional EE% reflects the advantageous structural architecture of NLCs, wherein the deliberate imperfection in the lipid crystalline matrix achieved by blending solid lipids (glyceryl monostearate and Compritol® 888 ATO) with liquid lipid (medium-chain triglycerides) creates additional void spaces that accommodate drug molecules more effectively than conventional solid lipid nanoparticles. The high drug loading of approximately 9.5% is particularly significant for pulmonary delivery applications, as it enables therapeutically relevant doses to be delivered with minimal carrier mass, thereby reducing the total aerosolized particle burden while maintaining efficacy. The verification experiment confirmed 98.7% drug recovery, validating that the ultrafiltration-centrifugation method did not compromise NLC integrity and that the membrane exhibited negligible nonspecific binding to free FP, as evidenced by the 98.2% recovery in preliminary validation studies.

*In Vitro Aerosolization Performance*

The aerosolization characteristics of FP-NLCs, evaluated using a Pari LC Plus nebulizer coupled with a next-generation impactor (NGI), are presented in Table 3. The formulation exhibited an emitted dose of 87.4 ± 1.8%, indicating minimal drug retention within the nebulizer cup and tubing a critical parameter for ensuring that the nominal dose reaches the patient's respiratory tract. More importantly, the fine particle fraction (FPF) of 68.3 ± 2.4% substantially exceeded that of the free FP solution control (42.6 ± 3.1%), demonstrating that NLC encapsulation significantly enhances deposition in the deep lung region (stages 3–7, corresponding to aerodynamic diameters <4.46

Table 3. In Vitro Aerosolization Performance of Inhalable FP-NLCs via Nebulizer-NGI System.

| Aerosolization Parameter | FP-NLC Formulation | Free FP Solution (Control) |
|---|---|---|
| Emitted Dose (ED, %) | 87.4 ± 1.8 | 91.2 ± 2.1 |
| Fine Particle Fraction (FPF, %) | 68.3 ± 2.4 | 42.6 ± 3.1 |
| Mass Median Aerodynamic Diameter (MMAD, μm) | 2.87 ± 0.15 | 3.94 ± 0.22 |
| Geometric Standard Deviation (GSD) | 1.82 ± 0.00 | 1.95 ± 0.03 |
| Fine Particle Dose (FPD, μg) | 341.5 ± 12.7 | 213.0 ± 15.6 |
| Total Drug Recovered from NGI (%) | 89.1 ± 1.5 | 92.3 ± 1.8 |

μm). The mass median aerodynamic diameter (MMAD) of 2.87 ± 0.15 μm falls within the optimal range of 1–5 μm for alveolar deposition, whereas the free FP solution displayed a larger MMAD of 3.94 μm, suggesting that NLC formulation produces finer, more respirable aerosols. This improvement can be attributed to the reduced surface tension and enhanced colloidal stability of NLC dispersions during nebulization, which prevent droplet coalescence and generate narrower particle size distributions, as evidenced by the lower geometric standard deviation (GSD = 1.82 vs. 1.95). The fine particle dose (FPD) of 341.5 μg for FP-NLCs versus 213.0 μg for free FP further confirms that encapsulation delivers approximately 60% more drug to the alveolar region, which is clinically significant for treating chronic inflammatory respiratory diseases such as asthma and COPD.

*In Vitro Release Kinetics*

The drug release profiles of FP from NLCs, shown in Table 4, reveal a sustained and controlled release pattern extending over 48 hours, in stark contrast to the rapid release (>99% within 4 hours) observed for free FP solution. The FP-NLC formulation exhibited an initial burst release of 8.2% within 0.25 hours, followed by a gradual, prolonged release reaching 95.8% at 48 hours. This biphasic release behavior is characteristic of lipid nanocarriers, where the initial burst corresponds to drug molecules adsorbed on the NLC surface or located in less ordered regions of the lipid matrix, while the sustained phase reflects drug diffusion from the nanoparticle core. The kinetic modeling analysis (Table 4) demonstrated that the Korsmeyer-Peppas model provided the best fit ($R^2$ = 0.9912, AIC = 31.2), with a release exponent (n) of 0.67 ± 0.03. This n value falls within the range of 0.45 < n < 0.89, indicating anomalous (non-Fickian) transport, wherein drug release is governed by both diffusion through the lipid matrix and erosion/relaxation of the carrier itself. The Higuchi model also showed good correlation ($R^2$ = 0.9834), further supporting diffusion-controlled release as a dominant mechanism. This sustained release profile is therapeutically advantageous for chronic respiratory diseases, as it maintains therapeutic drug concentrations in the lung lining fluid for extended periods, potentially reducing dosing frequency and improving patient compliance while minimizing systemic exposure and associated corticosteroid side effects. The prolonged pulmonary retention achieved by FP-NLCs aligns with previous findings that nanoparticulate systems decrease mucociliary clearance and enable dissolution rate-limited absorption, thereby extending local anti-inflammatory efficacy.

Together, these results establish that inhalable FP-NLCs combine high encapsulation efficiency, optimal aerodynamic properties for deep lung

Table 4. In Vitro Drug Release Kinetics of FP from Optimized NLCs and Kinetic Model Parameters.

| Time Point (h) | Cumulative Release (%) FP-NLC | Cumulative Release (%) Free FP Control |
|---|---|---|
| 0.25 | 8.2 ± 0.4 | 42.5 ± 1.2 |
| 0.5 | 15.7 ± 0.6 | 68.3 ± 1.8 |
| 1 | 26.4 ± 0.8 | 89.7 ± 2.1 |
| 2 | 38.9 ± 1.1 | 97.2 ± 1.5 |
| 4 | 52.3 ± 1.3 | 98.8 ± 0.9 |
| 6 | 61.8 ± 1.5 | 99.4 ± 0.7 |
| 8 | 69.5 ± 1.7 | 99.7 ± 0.5 |
| 12 | 78.2 ± 1.9 | 99.9 ± 0.3 |
| 24 | 87.6 ± 2.1 | — |
| 36 | 92.4 ± 2.3 | — |
| 48 | 95.8 ± 2.5 | — |

Table 5. Kinetic Model Fitting Parameters for FP-NLC.

| Kinetic Model | Equation | $R^2$ | AIC | Release Exponent (n) |
|---|---|---|---|---|
| Zero-order | Q = Q~0~ + kt | 0.9421 | 48.7 | — |
| First-order | ln(Q~∞~ − Q) = lnQ~∞~ − kt | 0.9687 | 42.3 | — |
| Higuchi | Q = k~H~t^0.5^ | 0.9834 | 36.8 | — |
| Korsmeyer-Peppas | Q/Q~∞~ = kt^n^ | 0.9912 | 31.2 | 0.67 ± 0.03 |

deposition, and sustained release kinetics three critical attributes for successful pulmonary delivery of anti-inflammatory drugs in chronic respiratory diseases.

*Comprehensive Discussion, Limitations, and Future Perspectives*

The experimental findings presented in this study collectively demonstrate that nanostructured lipid carriers (NLCs) represent a viable and potentially superior platform for the pulmonary delivery of anti-inflammatory drugs, specifically fluticasone propionate, in the context of chronic respiratory diseases. The FE-SEM micrographs (Fig. 1) confirmed that the optimized formulation yields spherical, non-aggregated nanoparticles with a mean diameter of approximately 128 nm, a size range that is widely regarded as optimal for evading rapid mucociliary clearance and alveolar macrophage recognition while still depositing efficiently in the deeper lung regions. The FT-IR spectra (Fig. 2) provided compelling evidence that the drug remains molecularly dispersed within the disordered lipid matrix rather than crystallizing on the particle surface, a finding that was further substantiated by the TGA thermograms (Fig. 3), which showed no independent degradation event corresponding to free drug. Taken together, these physicochemical characterizations paint a consistent picture: the NLCs successfully encapsulate and stabilize a lipophilic anti-inflammatory agent through weak, reversible hydrophobic interactions, thereby preserving the chemical integrity of both the drug and the lipid excipients.

When considering the broader implications of this work, several points merit deeper reflection. First, the use of a blend of solid lipids (GMS and Compritol® 888 ATO) with a liquid lipid (MCT) in a 70:30 ratio appears to strike an effective balance between structural rigidity and drug accommodation capacity. The imperfect crystal type NLCs generated by this composition provide sufficient lattice defects to house the FP molecules without expelling them during storage, a problem that frequently plagued first-generation solid lipid nanoparticles. Second, the choice of Poloxamer 188 and TPGS as surfactant co-stabilizers is not arbitrary: the former provides steric stabilization and biocompatibility, while the latter a PEGylated vitamin E derivative offers the additional advantage of inhibiting P-glycoprotein efflux pumps, which may be relevant if any portion of the drug reaches the systemic circulation or if the formulation is repurposed for other hydrophobic drugs. This dual-surfactant strategy could prove particularly valuable for chronic respiratory diseases such as asthma or chronic obstructive pulmonary disease (COPD), where long-term, sustained anti-inflammatory action is desired without frequent dosing.

Nevertheless, the present study is not without its limitations, and acknowledging these openly is essential for guiding future investigations. One notable constraint is that all characterizations were performed under static, in vitro conditions. While FE-SEM, FT-IR, and TGA provide invaluable information about particle morphology, chemical compatibility, and thermal stability, they do not replicate the dynamic, humid, and shear-intensive environment of the human respiratory tract. During actual nebulization, the NLCs will encounter air–liquid interfaces, variable surface tensions, and potential interactions with lung surfactants such as dipalmitoylphosphatidylcholine (DPPC). It remains unknown whether these physiological factors could trigger drug leakage, particle aggregation, or premature release before the carriers reach the alveolar epithelium. Future studies should therefore incorporate more biomimetic models, such as the Calu3 air–liquid interface cell culture system or ex vivo perfused lung models, to better approximate in vivo performance.

Another limitation concerns the absence of long-term stability data. Although the TGA results suggest adequate thermal robustness, they do not address the physical stability of the NLC dispersion over the course of weeks or months under recommended storage conditions (typically 4 °C for aqueous lipid nanoparticle dispersions). Issues such as Ostwald ripening, lipid polymorphic transitions from the less stable α-form to the more crystalline β-form, and hydrolytic degradation of ester linkages could gradually compromise encapsulation efficiency and aerosolization performance. We therefore recommend that future work include accelerated stability studies according to ICH guidelines (e.g., 25 °C/60 % RH and 40 °C/75 % RH for up to six months), complemented by monitoring of particle size, polydispersity index, zeta potential, and drug leakage at regular intervals.

A third limitation lies in the scope of anti-inflammatory efficacy evaluation. While we

focused on physicochemical characterization a necessary first step no cellular or animal data were collected to confirm that the FP-loaded NLCs retain pharmacological activity, achieve sustained local concentrations in lung tissues, or reduce inflammatory biomarkers such as tumor necrosis factorα (TNFα), interleukin6 (IL6), or leukotriene B4 (LTB4). Without such biological validation, the translational potential of these NLCs remains speculative. Given that chronic respiratory diseases involve complex interplay between epithelial cells, macrophages, and recruited neutrophils, future investigations should employ lipopolysaccharide (LPS)-stimulated macrophage cell lines (e.g., RAW 264.7 or MH-S) to quantify the anti-inflammatory effect of encapsulated FP relative to free drug. Furthermore, in vivo biodistribution studies using fluorescently labeled NLCs in murine models of LPSinduced lung inflammation would provide critical information about residence time, tissue penetration, and avoidance of systemic absorption.

Looking toward future directions, several promising avenues emerge from the current work. First, the NLC platform could be adapted for combination therapy by co-encapsulating two or more anti-inflammatory agents with complementary mechanisms of action for example, a corticosteroid paired with a long-acting betaagonist (LABA) or a phosphodiesterase4 inhibitor. Such combinations are already standard in clinical practice for COPD and severe asthma, but delivering them within a single NLC formulation could simplify treatment regimens and potentially achieve synergistic effects at lower individual doses. Second, the surface chemistry of the NLCs could be further refined by conjugating targeting ligands such as mannose or folic acid to enhance selective uptake by alveolar macrophages (which express mannose receptors) or by epithelial cells in inflamed regions (which overexpress folate receptors). Active targeting could reduce the required dose and minimize off-target effects. Third, the formulation could be converted into a dry powder for inhalation by spray drying or lyophilization with suitable carriers (e.g., lactose or mannitol), thereby circumventing the stability issues associated with aqueous dispersions and offering compatibility with existing dry powder inhalers (DPIs). Fourth, the incorporation of stimuli-responsive lipids that degrade in the presence of reactive oxygen species (ROS) or elevated glutathione levels both characteristic of inflamed lung tissue could enable on-demand drug release precisely at the sites of active inflammation, further enhancing therapeutic efficacy while reducing systemic side effects.

From a regulatory and clinical translation perspective, several hurdles remain to be addressed before inhalable NLCs can reach patients. The lack of standardized protocols for assessing nanoparticle aerosol performance across different nebulizer types (jet, ultrasonic, vibrating mesh) and the absence of harmonized acceptance criteria for particle size distributions in the respirable range represent significant barriers to inter-laboratory comparability. Additionally, the potential for long-term accumulation of non-biodegradable lipid materials in the alveolar space even if the lipids are generally recognized as safe warrants careful toxicological evaluation through repeated-dose inhalation studies in appropriate animal models. Encouragingly, many of the lipids used in this study (GMS, Compritol, MCT, Poloxamer 188, TPGS) have established safety profiles in orally or parenterally administered pharmaceutical products, but their pulmonary safety profile is less well documented. Future safety assessments should include bronchoalveolar lavage fluid analysis (total protein, lactate dehydrogenase activity, and inflammatory cell counts) and histopathological examination of lung tissues after sub-chronic dosing.

In conclusion, the current study establishes a solid physicochemical foundation for the development of inhalable NLCs loaded with anti-inflammatory drugs, demonstrating favorable morphology, drug-matrix compatibility, and thermal stability. However, the translation of this platform into a clinically useful therapy will require rigorous biological validation, extended stability testing, and the implementation of advanced formulation strategies such as active targeting or stimuli-responsive release. By systematically addressing the limitations outlined above and pursuing the proposed future directions, nanostructured lipid carriers have the potential to evolve from a promising laboratory concept into a practical, patient-friendly intervention for chronic respiratory diseases an area that remains in urgent need of more effective and better-tolerated treatment options.

## CONCLUSION

In the present study, we successfully

developed and systematically characterized inhalable nanostructured lipid carriers loaded with fluticasone propionate (FP-NLCs) as a potential platform for the sustained pulmonary delivery of anti-inflammatory drugs in chronic respiratory diseases. The optimized formulation, prepared by hot high-pressure homogenization followed by ultrasonication, yielded spherical nanoparticles with a mean diameter of 128 ± 18 nm, as confirmed by FE-SEM analysis. FT-IR spectroscopy demonstrated the absence of chemical incompatibilities between the drug and lipid excipients, indicating molecular dispersion of FP within the nanostructured matrix, while TGA thermograms revealed enhanced thermal stability of the drug-loaded carriers compared to blank NLCs. The formulation achieved a high encapsulation efficiency of 95.3 ± 0.2 % and a drug loading of 9.53 ± 0.02 %, reflecting the advantage of the imperfect crystal matrix created by blending solid and liquid lipids. Aerosolization studies using a next-generation impactor coupled with a Pari LC Plus nebulizer showed a fine particle fraction of 68.3 ± 2.4 % and a mass median aerodynamic diameter of 2.87 ± 0.15 µm, confirming optimal deep lung deposition potential. In vitro release kinetics followed a sustained biphasic profile over 48 hours, with Korsmeyer-Peppas modeling indicating an anomalous (non-Fickian) transport mechanism (n = 0.67), suggesting that drug release is governed by both diffusion and matrix erosion. Collectively, these findings establish that FP-NLCs combine favorable morphological characteristics, chemical compatibility, thermal robustness, high encapsulation efficiency, optimal aerosolization behavior, and sustained release kinetics. While further biological validation, long-term stability assessment, and in vivo studies remain necessary, the present work provides a solid physicochemical foundation for the development of inhalable NLCs as a promising therapeutic intervention for chronic inflammatory respiratory conditions such as asthma and COPD.

## CONFLICT OF INTEREST

The authors declare that there is no conflict of interests regarding the publication of this manuscript.

## REFERENCES


1. Samimi S, Maghsoudnia N, Eftekhari RB, Dorkoosh F. Lipid-Based Nanoparticles for Drug Delivery Systems. Characterization and Biology of Nanomaterials for Drug Delivery: Elsevier; 2019:.47-76.
2. Kumar R. Lipid-Based Nanoparticles for Drug-Delivery Systems. Nanocarriers for Drug Delivery: Elsevier; 2019:249-284.
3. Waheed I, Ali A, Tabassum H, Khatoon N, Lai W-F, Zhou X. Lipid-based nanoparticles as drug delivery carriers for cancer therapy. Front Oncol. 2024;14.
4. Gandhi S, Shastri DH. Lipid-based Nanoparticles as Drug Delivery System for Modern Therapeutics. Pharmaceutical Nanotechnology. 2026;14(1):1-28.
5. Plaza-Oliver M, Santander-Ortega MJ, Lozano MV. Current approaches in lipid-based nanocarriers for oral drug delivery. Drug Delivery and Translational Research. 2021;11(2):471-497.
6. Patel D, Patel B, Thakkar H. Lipid Based Nanocarriers: Promising Drug Delivery System for Topical Application. Eur J Lipid Sci Technol. 2021;123(5).
7. Okonogi S, Riangjanapatee P. Potential technique for tiny crystalline detection in lycopene-loaded SLN and NLC development. Drug Development and Industrial Pharmacy. 2013;40(10):1378-1385.
8. Andonova V, Peneva P. Characterization Methods for Solid Lipid Nanoparticles (SLN) and Nanostructured Lipid Carriers (NLC). Curr Pharm Des. 2018;23(43):6630-6642.
9. Das S, Ng WK, Tan RBH. Are nanostructured lipid carriers (NLCs) better than solid lipid nanoparticles (SLNs): Development, characterizations and comparative evaluations of clotrimazole-loaded SLNs and NLCs? Eur J Pharm Sci. 2012;47(1):139-151.
10. Nafee N, Makled S, Boraie N. Nanostructured lipid carriers versus solid lipid nanoparticles for the potential treatment of pulmonary hypertension via nebulization. Eur J Pharm Sci. 2018;125:151-162.
11. Sherif AY, Harisa GI, Alanazi FK, Nasr FA, Alqahtani AS. PEGylated SLN as a Promising Approach for Lymphatic Delivery of Gefitinib to Lung Cancer. International Journal of Nanomedicine. 2022;Volume 17:3287-3311.
12. Yoon G, Park JW, Yoon I-S. Solid lipid nanoparticles (SLNs) and nanostructured lipid carriers (NLCs): recent advances in drug delivery. Journal of Pharmaceutical Investigation. 2013;43(5):353-362.
13. Chettupalli AK, Kakkerla A, Jadi RK, Uppu P, Ghazwani M, Hani U, et al. Design, development, and preclinical evaluation of pirfenidone-loaded nanostructured lipid carriers for pulmonary delivery. Sci Rep. 2025;15(1).
14. Pardeike J, Weber S, Zarfl HP, Pagitz M, Zimmer A. Itraconazole-loaded nanostructured lipid carriers (NLC) for pulmonary treatment of aspergillosis in falcons. Eur J Pharm Biopharm. 2016;108:269-276.
15. Pardeike J, Weber S, Haber T, Wagner J, Zarfl HP, Plank H, et al. Development of an Itraconazole-loaded nanostructured lipid carrier (NLC) formulation for pulmonary application. Int J Pharm. 2011;419(1-2):329-338.
16. K. K SP, Narayansamy D. Advancements in nanotechnology for targeted drug delivery in idiopathic pulmonary fibrosis: a focus on solid lipid nanoparticles and nanostructured lipid carriers. Drug Development and Industrial Pharmacy. 2025;51(4):285-294.
17. Gupta C, Jaipuria A, Gupta N. Inhalable Formulations to Treat Non-Small Cell Lung Cancer (NSCLC): Recent Therapies and Developments. Pharmaceutics. 2022;15(1):139.
18. Almurshedi AS, Aljunaidel HA, Alquadeib B, Aldosari BN, Alfaqiah IM, Almarshidy SS, et al. Development of Inhalable Nanostructured Lipid Carriers for Ciprofloxacin for Noncystic Fibrosis Bronchiectasis Treatment. International Journal of Nanomedicine. 2021;Volume 16:2405-2417.
19. Ara N, Hafeez A, Kushwaha SP, Kapoor A. Inhalable Microparticles of Simvastatin-Loaded Nanostructured Lipid Carriers for Lung Cancer Treatment: Drug Delivery Development, In Vitro Characterization, and In Vivo Evaluation. BioNanoScience.

2026;16(4).
20. Salvi VR, Pawar P. Nanostructured lipid carriers (NLC) system: A novel drug targeting carrier. J Drug Deliv Sci Technol. 2019;51:255-267.
21. Müller RH, Radtke M, Wissing SA. Solid lipid nanoparticles (SLN) and nanostructured lipid carriers (NLC) in cosmetic and dermatological preparations. Adv Drug Del Rev. 2002;54:S131-S155.
22. Müller RH, Alexiev U, Sinambela P, Keck CM. Nanostructured Lipid Carriers (NLC): The Second Generation of Solid Lipid Nanoparticles. Percutaneous Penetration Enhancers Chemical Methods in Penetration Enhancement: Springer Berlin Heidelberg; 2016. p. 161-185. http://dx.doi.org/10.1007/978-3-662-47862-2_11
23. Muller R, Petersen R, Hommoss A, Pardeike J. Nanostructured lipid carriers (NLC) in cosmetic dermal products. Adv Drug Del Rev. 2007;59(6):522-530.
24. Pyo S-M, Müller RH, Keck CM. Encapsulation by nanostructured lipid carriers. Nanoencapsulation Technologies for the Food and Nutraceutical Industries: Elsevier; 2017. p. 114-137. http://dx.doi.org/10.1016/b978-0-12-809436-5.00004-5
25. Mirantsev LV, de Oliveira EJL, de Oliveira IN, Lyra ML. Defect structures in nematic liquid crystal shells of different shapes. Liquid Crystals Reviews. 2016;4(1):35-58.
26. Tarnavskyy OS, Ledney MF. Equilibrium locations of defects in two-dimensional configurations of the NLC director field. Liq Cryst. 2022;50(1):21-35.
27. Gordillo-Galeano A, Ponce A, Mora-Huertas CE. In vitro release behavior of SLN, NLC, and NE: An explanation based on the particle structure and carried molecule location. J Drug Deliv Sci Technol. 2022;76:103768.
28. Javed S, Mangla B, Almoshari Y, Sultan MH, Ahsan W. Nanostructured lipid carrier system: A compendium of their formulation development approaches, optimization strategies by quality by design, and recent applications in drug delivery. Nanotechnology Reviews. 2022;11(1):1744-1777.
29. Tetyczka C, Griesbacher M, Absenger-Novak M, Fröhlich E, Roblegg E. Development of nanostructured lipid carriers for intraoral delivery of Domperidone. Int J Pharm. 2017;526(1-2):188-198.
30. Chen PC, Huang J-W, Pang J. An Investigation of Optimum NLC-Sunscreen Formulation Using Taguchi Analysis. Journal of Nanomaterials. 2013;2013(1).
31. Khan S, Sharma A, Jain V. An Overview of Nanostructured Lipid Carriers and its Application in Drug Delivery through Different Routes. Advanced Pharmaceutical Bulletin. 2022;13(3):446-460.
32. Jansook P, Fülöp Z, Ritthidej GC. Amphotericin B loaded solid lipid nanoparticles (SLNs) and nanostructured lipid carrier (NLCs): physicochemical and solid-solution state characterizations. Drug Development and Industrial Pharmacy. 2019;45(4):560-567.
33. Teeranachaideekul V, Muller R, Junyaprasert V. Encapsulation of ascorbyl palmitate in nanostructured lipid carriers (NLC)—Effects of formulation parameters on physicochemical stability. Int J Pharm. 2007;340(1-2):198-206.
34. Jafarifar Z, Rezaie M, Sharifan P, Jahani V, Daneshmand S, Ghazizadeh H, et al. Preparation and Characterization of Nanostructured Lipid Carrier (NLC) and Nanoemulsion Containing Vitamin D3. Applied Biochemistry and Biotechnology. 2021;194(2):914-929.
35. Vieira R, Severino P, Nalone LA, Souto SB, Silva AM, Lucarini M, et al. Sucupira Oil-Loaded Nanostructured Lipid Carriers (NLC): Lipid Screening, Factorial Design, Release Profile, and Cytotoxicity. Molecules. 2020;25(3):685.
36. Yostawonkul J, Surassmo S, Iempridee T, Pimtong W, Suktham K, Sajomsang W, et al. Surface modification of nanostructure lipid carrier (NLC) by oleoyl-quaternized-chitosan as a mucoadhesive nanocarrier. Colloids Surf B Biointerfaces. 2017;149:301-311.
37. Binici B, Rattray Z, Zinger A, Perrie Y. Exploring the impact of commonly used ionizable and pegylated lipids on mRNA-LNPs: A combined in vitro and preclinical perspective. Journal of Controlled Release. 2025;377:162-173.
38. Park S, Choi YK, Kim S, Lee J, Im W. CHARMM-GUI Membrane Builder for Lipid Nanoparticles with Ionizable Cationic Lipids and PEGylated Lipids. J Chem Inf Model. 2021;61(10):5192-5202.
39. Roces CB, Lou G, Jain N, Abraham S, Thomas A, Halbert GW, et al. Manufacturing Considerations for the Development of Lipid Nanoparticles Using Microfluidics. Pharmaceutics. 2020;12(11):1095.
40. Ahmed R, Tewes F, Aucamp M, Dube A. Formulation and clinical translation of inhalable nanomedicines for the treatment and prevention of pulmonary infectious diseases. Drug Delivery and Translational Research. 2025;15(9):2967-2993.
41. Mohini K, Shabnam T, Sharma R, Sharma S. Translation of lipid based formulation for pulmonary drug delivery system: Clinical status. Lipids in Pulmonary Drug Delivery: Elsevier; 2025. p. 371-396. http://dx.doi.org/10.1016/b978-0-443-22374-7.00017-7
42. Kumar A, Dailey LA, Forbes B. Lost in Translation: What is Stopping Inhaled Nanomedicines From Realizing Their Potential? Ther Deliv. 2014;5(7):757-761.
43. Gomaa E, Fathi HA, Eissa NG, Elsabahy M. Methods for preparation of nanostructured lipid carriers. Methods. 2022;199:3-8.
44. Hu F-Q, Jiang S-P, Du Y-Z, Yuan H, Ye Y-Q, Zeng S. Preparation and characteristics of monostearin nanostructured lipid carriers. Int J Pharm. 2006;314(1):83-89.
45. Duong V-A, Nguyen T-T-L, Maeng H-J. Preparation of Solid Lipid Nanoparticles and Nanostructured Lipid Carriers for Drug Delivery and the Effects of Preparation Parameters of Solvent Injection Method. Molecules. 2020;25(20):4781.
46. Lin X, Li X, Zheng L, Yu L, Zhang Q, Liu W. Preparation and characterization of monocaprate nanostructured lipid carriers. Colloids Surf Physicochem Eng Aspects. 2007;311(1-3):106-111.
47. Kasongo KW, Müller RH, Walker RB. The use of hot and cold high pressure homogenization to enhance the loading capacity and encapsulation efficiency of nanostructured lipid carriers for the hydrophilic antiretroviral drug, didanosine for potential administration to paediatric patients. Pharmaceutical Development and Technology. 2011;17(3):353-362.
48. Wu K-W, Sweeney C, Dudhipala N, Lakhani P, Chaurasiya ND, Tekwani BL, et al. Primaquine Loaded Solid Lipid Nanoparticles (SLN), Nanostructured Lipid Carriers (NLC), and Nanoemulsion (NE): Effect of Lipid Matrix and Surfactant on Drug Entrapment, in vitro Release, and ex vivo Hemolysis. AAPS PharmSciTech. 2021;22(7).
49. How CW, Rasedee A, Manickam S, Rosli R. Tamoxifen-loaded nanostructured lipid carrier as a drug delivery system: Characterization, stability assessment and cytotoxicity. Colloids Surf B Biointerfaces. 2013;112:393-399.
50. Patil-Gadhe A, Kyadarkunte A, Patole M, Pokharkar V. Montelukast-loaded nanostructured lipid carriers: Part II Pulmonary drug delivery and in vitro–in vivo aerosol performance. Eur J Pharm Biopharm. 2014;88(1):169-177.
51. Ortiz AC, Yañez O, Salas-Huenuleo E, Morales JO. Development of a Nanostructured Lipid Carrier (NLC) by a Low-Energy Method, Comparison of Release Kinetics and Molecular Dynamics Simulation. Pharmaceutics. 2021;13(4):531.
52. Sadati Behbahani E, Ghaedi M, Abbaspour M, Rostamizadeh K, Dashtian K. Curcumin loaded nanostructured lipid carriers: In vitro digestion and release studies. Polyhedron. 2019;164:113-122.